Multipath Exploitation for Human Activity Recognition using a Radar Network

Guendel, Ronny G.; Kruse, Nicolas C.; Fioranelli, Francesco; Yarovoy, Alexander

DOI
10.1109/TGRS.2024.3363631

Publication date
2024

Document Version
Final published version

Published in
IEEE Transactions on Geoscience and Remote Sensing

Multipath Exploitation for Human Activity Recognition Using a Radar Network

Ronny Gerhard Guendel, *Graduate Student Member, IEEE*,
Nicolas C. Kruse, *Graduate Student Member, IEEE*,
Francesco Fioranelli, *Senior Member, IEEE*,
and Alexander Yarovoy, *Fellow, IEEE*

***Abstract*— In this study, the problem of multipath in radar sensor networks for human activity recognition (HAR) has been examined. Traditionally considered as a source of additional clutter, the multipath is being investigated for its potential to be exploited through the creation of virtual radar nodes. These virtual nodes are conceptualized to observe targets from aspect angles that differ from those of physically existing radars. To realize this idea, an innovative processing pipeline is proposed that extracts information from multipath signals to improve HAR. The pipeline isolates and tracks the line-of-sight (LOS) and multipath components of a moving human target performing continuous sequences of activities observed by a network of three radar sensors. Furthermore, the method has been verified with experimental data consisting of six activities and 14 volunteers by comparing classification metrics with the use of a single radar as well as only the LOS components of the three radars in the network. A 12-layer convolutional neural network (CNN) classifier has been designed to operate on range-Doppler (RD) images derived from the LOS and multipath components, extracted by the proposed method. A substantial performance improvement using the leave-one-person-out (L1Po) test set is demonstrated in the order of +11% by exploiting a multiradar network with its LOS and multipath components.**

***Index Terms*— Clustering, distributed radar, hierarchical clustering, human activity recognition (HAR), multilateration, multipath, radar multipath, radar signal processing, trilateration.**

I. Introduction

RADAR sensor networks can increase the efficacy of perception by leveraging diverse observations from multiple radar nodes. Applications of radar networks include nonintrusive monitoring and activity classification, especially of vulnerable individuals in case of falls or other potentially dangerous events among other daily activities [1], [2].

Existing literature on human activity classification from radar measurements primarily characterizes the received signal with micro-Doppler or range-Doppler (RD) signatures of a radar's line-of-sight (LOS) signal. In principle, Doppler modulations from micro-motions were found to have a substantial predictive impact on classification performances, with the benefits of using networks over single radar observations [3], [4], [5], [6]. Some studies have also introduced ensemble learning methods using a sensor network with boosted, bagged, and stacked machine learning (ML) models [7].

Although, researchers often utilize publicly available data [8], [9], [10], [11], focusing predominantly on classifier architectures and their deep learning variants [12], [13], [14], whereas they often do not include multipath and focus on other topics. Recently, attention has shifted to observing continuous sequences of activities in human kinematics [15], benefiting from the multiperspective views inherently offered by radar networks [16]. Some studies even incorporate in the network RF-based illuminators of opportunities widely available in consumer home environments, even if they may be affected by multipath and provide by themselves lower performances compared to their active counterparts [17], [18]. Examples of high-quality micro-Doppler signatures that use, for example, passive Wi-Fi in the context of human activity recognition (HAR) and hand gesture recognition, have been reported [19], [20].

In the introduced literature on human activity classification with single, monostatic radars or radar networks, multipath is often considered as an unwanted phenomenon degrading the overall performance of the system. However, in some cases, multipath components can be exploited to improve indoor localization, as shown for monostatic setups [21] and for multi-in–multioutput (MIMO) radar applications of point targets [22], [23]. Inspired by the concepts presented in those studies, a novel processing pipeline is introduced, which enables the exploitation of multipath components within a radar network to enhance the overall classification process.

The rationale of the proposed approach is that the LOS signal (0th component) reflected by a target and its 1st- and 2nd-order multipath components are not only capturing the target's signature from different aspect angles [12], [24], but they are also coherent with each other as they originate from the same radar. This is dissimilar to the findings using a multistatic sensor system [25]. The former provides additional sources of information to characterize the target's scattering behavior and movement pattern, as if the multipath components were additional physical radar sensors observing the

Manuscript received 7 June 2023; revised 22 November 2023; accepted 26 January 2024. Date of publication 7 February 2024; date of current version 16 February 2024. This work was supported in part by the Dutch Research Council (NWO) through the RAD-ART, Radar-aware Activity Recognition with Innovative Temporal Networks Project. *(Corresponding author: Ronny Gerhard Guendel.)*

This work involved human subjects or animals in its research. Approval of all ethical and experimental procedures and protocols was granted by TU Delft, HREC, under Application No. 1387.

The authors are with the MS3 Group, Department of Microelectronics, Delft University of Technology, 2628 CD Delft, The Netherlands (e-mail: r.gundel@tudelft.nl).

Digital Object Identifier 10.1109/TGRS.2024.3363631

target from different perspectives. Utilized in the context of a physical radar network with different nodes, the proposed pipeline allows for the potential "augmentation" of the network by adding the multipath components related to each physical radar node, which would typically be discarded in conventional processing. The proposed pipeline consists in short of the following steps, which will be detailed in the following.

1) The LOS component is established via a hierarchical clustering algorithm to deal with the extended nature of the human target due to the high spatial resolution of the radars used. This enables the isolation and tracking of the LOS and the multipath components in the range-time (RT) data.
2) The pipeline determines the location of the target via multilateration, as well as the locations of the generated multipath components as the target moves.
3) Features are extracted from RD images of each "data domain," which includes the LOS and the 1st- and 2nd-order multipath components, for each radar in the network.
4) ML classifiers are trained and tested on data for verification, which also includes the upsampling of the unbalanced data using the synthetic minority oversampling (SMOTE) technique proposed in [26] and [27].
5) A rigorous leave-one-person-out (L1Po) test is performed for the final verification of the classifiers.

It should be emphasized that SMOTE is helpful in the context of naturally unbalanced datasets [28] with continuously recorded sequences for HAR, as it can provide augmentation for minority classes. Unlike the common implementations of SMOTE on feature vectors, here the technique is also applied on image data, as proposed in others' work [27], [29].

More specifically, the proposed pipeline has been verified with experimental data collected with a network of three pulsed radar nodes. The data include six activities performed by 14 volunteers, used to compare different classification algorithms, namely, a support vector machine (SVM) classifier, a multilayer perceptron (MLP) classifier, and a convolutional neural network (CNN). The classification performances of the F1-score are shown to increase up to about +11% (with respect to using a monostatic radar node) thanks to the inclusion of data and features retrieved from the multipath components using the proposed processing pipeline.

The remainder of this article is organized as follows. The proposed pipeline is discussed in Section II with its signal processing architecture, target tracking, and ML models. The dataset with the participants' statistics and the obtained results can be found in Section III. Finally, conclusions and remarks for future work are given in Section IV.

II. Proposed Pipeline for Multipath Exploitation

Multipath is often considered as an undesired effect to be removed in radar applications, including indoor human activity classification. However, research in wireless communication has demonstrated the benefits of using multipath [21], [30] for improved localization. In this article, a novel processing pipeline is proposed to locate multipath components related to human movement in an indoor setting and exploit them for the classification process.

The rationale of using multipath components for classification is that they capture the target's signature from different spatial perspectives (aspect angle) and are coherent with the main LOS signal as generated by the same radar. This allows to consider the signature in the multipath components as if generated by additional physical radar nodes, thus enabling the exploitation of additional data for classification. A key task in the proposed pipeline is the identification of the LOS and multipath components from the RT data, and their tracking over time while the human target moves. The proposed processing pipeline is shown in the block diagram of Fig. 1 and is described in detail in the rest of this section.

A. LOS Isolation From Multipath Components

This section describes the proposed method for isolating the LOS from higher order multipath components using continuously recorded data from each radar node. It is essential to mention that multipaths can be modeled as a copy of the LOS backscattered signal since it is delayed with respect to the LOS, and thus, it appears at a further-off location. In many cases, the multipath arrives from different angles of arrival (AoAs) and with amplitudes lower than those of the LOS. To exploit the information in the multipath components, an essential step is separating the LOS signal from such multipath components and formulating a method to track these signals in the RT data. As seen in the RT map $\mathbf{M}$ in Fig. 2, a problem for such separation and tracking is that the target's backscattered signal does not follow a Gaussian distributed function $\mathcal{N}(\mu, \sigma^2)$ with mean, μ, and variance, σ^2 [31], as a result of the presence of multipath as well as the extended nature of the human target. A feasibility study with a constant velocity and constant acceleration tracking filter (not reported for conciseness) did not provide good results in isolating and extracting the LOS from the RT data.

Furthermore, a signal-to-noise ratio (SNR) analysis was carried out, taking as an example a portion of data where a person transitions from a walking state to a standing position, at approximately 1.25 m from the radar. In this analysis, the radar R3 was used, which is positioned on the reflector wall, as depicted in Fig. 3. The measured SNR was approximately 39.8 dB, whereas the signal-to-clutter ratio (SCR) was estimated to be in the range of 35.7 dB, as measured from recordings of the room background without moving participants in the scene. With the assumption that the radar-target LOS component is the spatially closest and oftentimes strongest component, the problem of its isolation is formulated via a hierarchical clustering algorithm (also known as agglomerative clustering) [32]. Different alternatives, including a multiple target tracking (MTT) approach [31] applied to the distinct propagation paths [33], were considered. Another powerful approach for indoor monitoring is the multiple hypotheses tracker (MHT), as demonstrated by Dogaru et al. [34] and also explored in other research works [35], [36]. However, the chosen hierarchical clustering method has shown superior results for an extended human target, as in

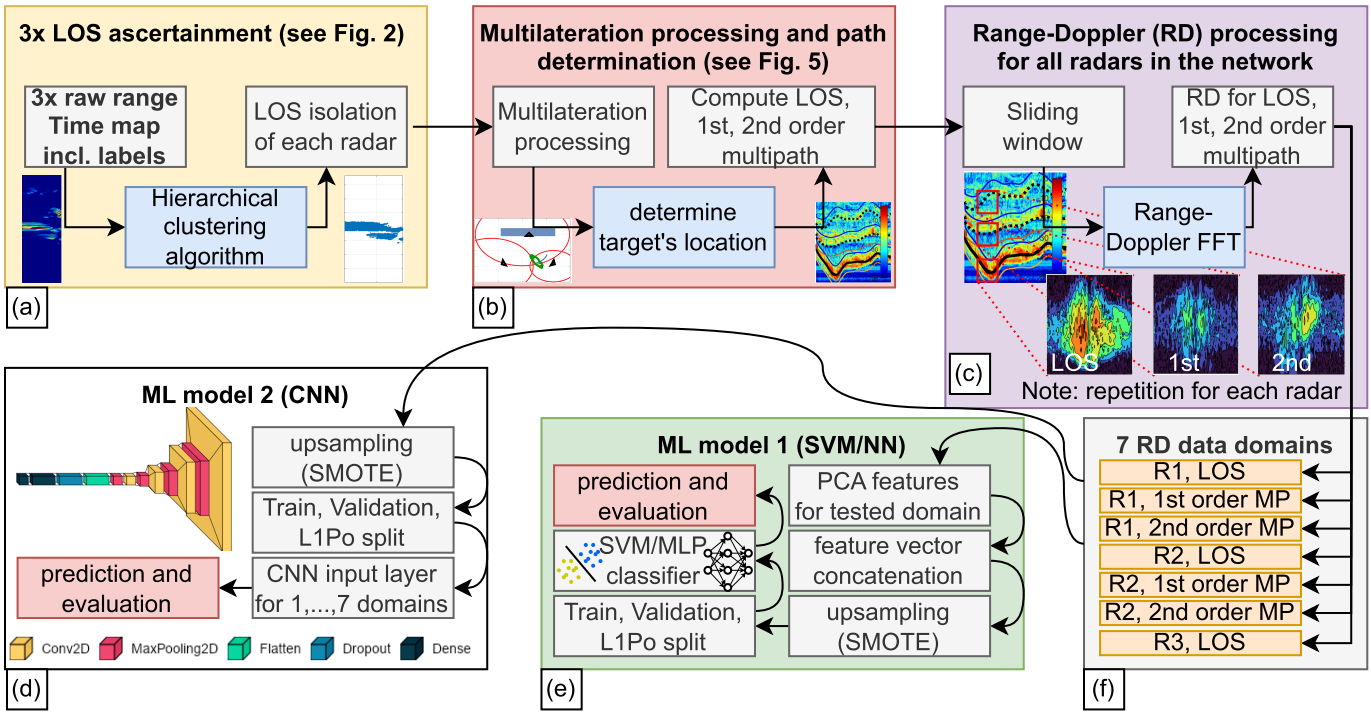

Fig. 1. Proposed processing pipeline for multipath exploitation in human activity classification (HAR) with two classifier pipelines tested. The blocks of (a) *LOS ascertainment*, and (b) *multilateration processing and path determination* are explained in more detail in Figs. 2 and 6, respectively, followed by the pipeline's blocks, (c) range-Doppler extraction, (f) data domain overview, (e) machine learning (ML) model 1 and (d) ML model 2.

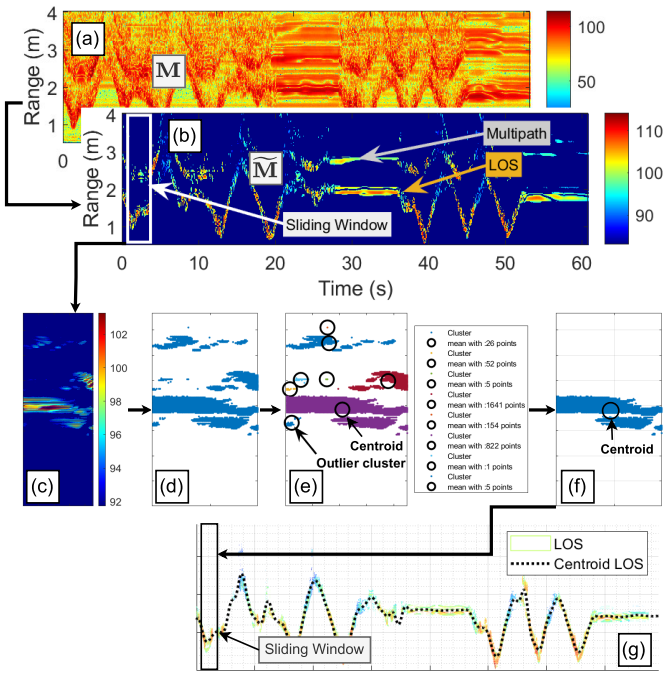

Fig. 2. Flowgraph providing insights from Fig. 1(a). (a) Initial RT map with LOS and multipath components, (b) selection of the k-strongest range bins, (c)–(f) clustering steps to delineate the LOS cluster from noise and multipath, and (g) refined RT map featuring the LOS signal and its centroid.

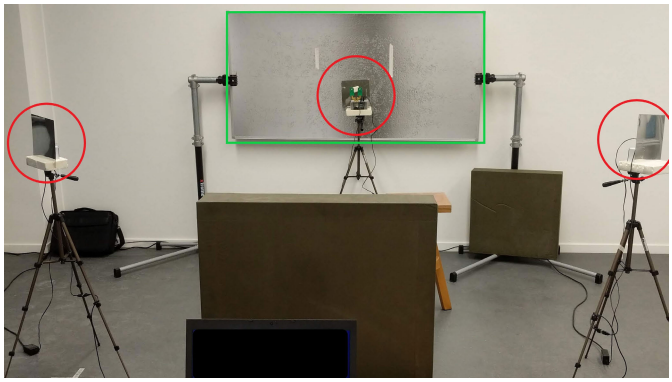

Fig. 3. Experimental setup showing the radar nodes circled in red and the reflector in the green rectangle. Additional geometry details can be found in Fig. 5(a).

the considered case, and this has the advantages of: 1) not requiring a predefined number of clusters and 2) being capable to account for arbitrary shapes of the clusters.

1) Hierarchical Clustering Algorithm: Hierarchical clustering requires the creation of clusters from the initial RT map, defined as a matrix $\mathbf{M} = \mathbf{S}_{\text{LOS}} + \mathbf{S}_{\text{multipaths}} + \mathbf{N}$, which includes the signals denoted by $\mathbf{S}_{\{\cdot\}}$ and the noise term $\mathbf{N}$. Therefore, as a preliminary step to identify the LOS component, the k-strongest range bins of the RT map are selected as follows:

$$\widetilde{\mathbf{M}}_{ij} = \begin{cases} \underset{i}{\text{argmax}}_{\,k}\ \mathbf{M}_{ij}, & k\text{-strongest} \\ 0, & \text{otherwise} \end{cases} \tag{1}$$

with i (fast time/range bins) the column and j (slow time) the row elements of the matrices $\mathbf{M}_{ij}$, forming the sparse matrix $\widetilde{\mathbf{M}}_{ij}$. This matrix mainly contains detected LOS components and some residuals of the multipath components, as shown in Fig. 2.

Then, slow-time windowing is performed with a window length of $3k$, with k being the parameter denoted earlier in (1) as the k-strongest samples. This parameter is the empirically determined optimal sample number to mitigate arbitrary connections between LOS and multipath clusters,

as shown in Fig. 2 with $3k = 90$ slow-time sample bins (equivalent to ≈0.74 s).

After applying the clustering algorithm, the separate clusters are typically represented using a Venn diagram, and then, the so-called dendrogram is used to specify the distances between the clusters [37]. Beyond the aforementioned k-strongest parameter, the implementation of the clustering algorithm also depends on the cutoff distance parameter, which provides the distances between the clusters calculated via the default Euclidean distance [32]. It should be noted that numerous clustering algorithms exist in the literature; the one chosen for this study was selected for its ability to: 1) process clusters of arbitrary shapes and 2) operate without a predefined number of clusters, as introduced earlier. As a next step, the clusters found are selected based on range, as shown in Fig. 2(e), assuming that the closest cluster is most likely to the LOS propagation path. Finally, an empirical condition is set—based on the quantity of cluster points—to exclude smaller cluster clouds, as shown in Fig. 2(e) as *outlier cluster*. If this condition is not met, the algorithm selects the following farthest cluster in fast time/range and then moves the sliding window in slow time. The found cluster with its centroid is recorded as the window moves and is used to generate the RT map that contains only the LOS signal.

To identify the optimal values for the two critical clustering parameters—the k-strongest parameter and the cutoff distance—an optimization problem was formulated, which is described in the following.

2) Parameter Optimization for Hierarchical Clustering: An optimization method was implemented based on the R^2-score evaluation metric to minimize the error between the ground truth position of the LOS path and its prediction, returned by the hierarchical clustering algorithm. Other, more complex methods such as the higher order metric for evaluating multiobject tracking (HOTA) might also assess the algorithm's performance [38] but were not considered for conciseness in this work. The parameters for the hierarchical clustering algorithm are optimized within the ranges: 1) cutoff distance: $\in [3,\ 10,\ 20,\ 100]$ and 2) k-strongest to obtain $\widetilde{\mathbf{M}}$: $\in [15,\ 30,\ 60,\ 120]$ by using the performance metric R^2-score. The R^2-score has the property $\mathbb{R} \in (-\infty, 1]$ and is typically used to evaluate similarities in regression problems. The combination of cutoff and k-strongest values that maximizes the R^2-score is calculated. Therefore, a brute-force optimization approach is chosen to test every parameter combination and monitor its results $[m, n] := [k\text{-strongest, cutoff}]$ as

$$r_i = y_i - \hat{y}_i \forall\ i \in (0, N-1)$$
$$R^2_{m,n} = 1 - \frac{\sum_i r_i^2}{\sum_i \left(y_i - \mathbb{E}[y]\right)^2} \tag{2}$$

with r_i the residual between y_i the ground truth, $\hat{y}_i$ the predicted sample, and $\mathbb{E}[y]$ the expected value (mean of the ground truth) [39]. It should be noted that the *LOS ground truth*, as shown in the example in Fig. 4(a), was hand-labeled for the purpose of this small-scale optimization problem, which is only performed once to tune the parameters. Taking into account all combinations, the optimum for the k-strongest samples was found to be 30 and a cutoff distance was found to be 10, as shown in Fig. 4(b). These parameters are then used throughout the following analysis.

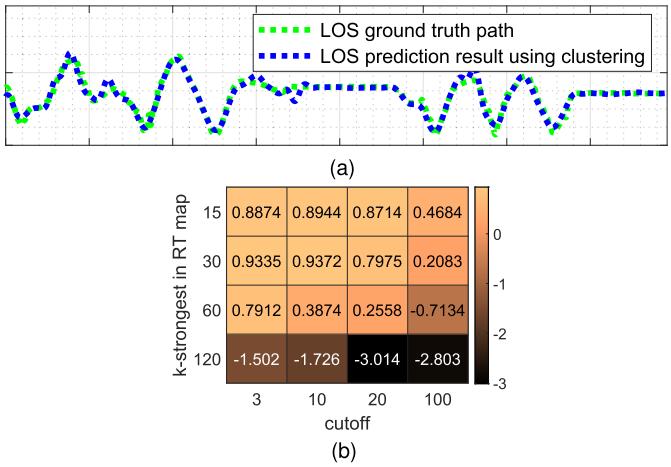

Fig. 4. Results of the clustering algorithm's parameter optimization. (a) Identified LOS path using the optimized parameters k-strongest = 30 and cutoff = 10, yielding an R^2-score of 93.72%. (b) R^2-scores obtained through a brute-force evaluation method.

B. Motivation Behind Multipath Modeling and Exploitation

After the LOS ranges were determined, multilateration processing was used to determine the target location over time. It should be noted that alternative approaches using an additional tracking filter, as in our previous work [40], can be implemented, whereas it is not considered for conciseness of this work.

After isolating the LOS path in the RT data, the multipath components can be reidentified using the known locations of the radars and the reflector, along with the determined target coordinates. A simple multipath model, as depicted in Fig. 5, is employed and further discussed in Section II-B2.

1) Multipath Model: The model considers a multipath-assisted localization (MAL) from 0th- (LOS) to 2nd-order reflections, as shown in the sketch of Fig. 5(a). A priori knowledge of the reflector's and radars' location is assumed. Specifically, as in the considered scenario, a network of three radar nodes is given, of which two—R1 and R2—can benefit from the multipath reflections created by the presence of a wall as a reflector of opportunity; the third radar is part of the network, but because of its position at the reflector wall, radar R3 does not benefit from multipath components.

The 0th-order component is essentially the LOS seen by the radars, indicated by the one-way range $r_{0,nx}$. The multipath component reflected on the wall is divided into two propagation segments $r_{1,nx}$ and $r_{2,nx}$. By fictive mirroring the radar on the reflector, the symmetrical equivalent of $r_{1,nx}$ becomes $r'_{1,nx}$ with the radar location $\mathbf{x}_{nx}$ becoming $\mathbf{x}'_{nx}$. This is shown in Fig. 5(b) for $\mathbf{x}_1$ and $\mathbf{x}'_1$. According to the geometrical relations, the propagation paths for the three dominant components can be determined as

$$\Gamma_{0,nx} = \frac{2 \cdot r_{0,nx}}{2} = r_{0,nx} \tag{3a}$$
$$\Gamma_{1,nx} = \frac{r_{0,nx} + r'_{1,nx} + r_{2,nx}}{2} \tag{3b}$$

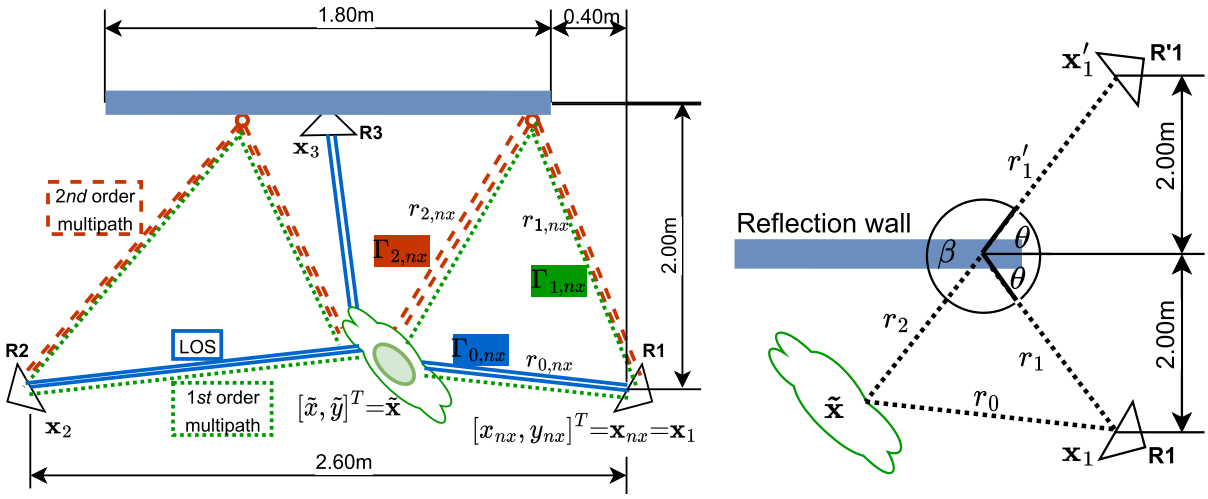

(a) Layout of the radar network with reflector (b) Fictive mirroring of radar node R1

Fig. 5. (a) Sketch of the room layout with three radars of which two radars—R1 and R2—can benefit from multipaths. R3 is placed on the reflection wall and provides the range for calculating the target location $\tilde{x}$ using trilateration. (b) Geometrical relationship to illustrate the multipath ranges, r_1, r_1', and r_2.

$$\Gamma_{2,nx} = \frac{2\cdot\left(r'_{1,nx}+r_{2,nx}\right)}{2} = r'_{1,nx}+r_{2,nx} \tag{3c}$$

with Γ being equal to half of the round-trip ranges, equivalent to the target's range in a typical RT map. The indices $\{\cdot\}_{0,\ldots,2,\{\cdot\}}$ are related to the 0th, 1st, and 2nd propagation paths, respectively, and $\{\cdot\}_{\{\cdot\},nx}$ denotes the radar node [21], [41], [42]. The emphasis is on using the different monostatic views of the 0th- (LOS) and 2nd-order multipath components, represented by $\Gamma_{0,nx}$ and $\Gamma_{2,nx}$, together with the bistatic views of the 1st-order multipath component (i.e., radar-wall-target-radar and vice versa, which are essentially the same due to reciprocity), denoted by $\Gamma_{1,nx}$, as shown in Fig. 5(a).

With this multipath model, the following characteristics can be expected for the scenario of interest.

1) For a human target, each component—LOS and 1st- and 2nd-order multipath—arrives at distinct time instants and appears typically in separate range cells, given the radar's high range resolution of approximately 68 mm [40].
2) The detected range cells occupied by the target's LOS (0th order) and 1st- and 2nd-order multipath components for a specific radar contain information about the same target, as a single target scenario is assumed.
3) Each radar's LOS and 1st- and 2nd-order multipath component captures the signature of the target from different aspect angles, conceptually equivalent to having additional physical radar nodes in the network.
4) The 1st-order multipath component acts as a bistatic propagation path, which enables to observe the scatter points of the target and their movements from a different perspective compared to the monostatic views of the LOS and 2nd-order multipath component.

2) Multilateration for LOS and Multipath Location Finding: Multilateration processing is applied to estimate the target's location in the radar network, as in [40]. Here, the LOS path extracted from the hierarchical clustering algorithm in Section II-A provides the radar-target's radial range $r_{0,nx}$, calculated with respect to the radar node with location $\mathbf{x}_{nx} = [x_{nx}, y_{nx}]^T$. The target's estimated position is denoted by $\tilde{x} = [\tilde{x}, \tilde{y}]^T$. For trilateration processing involving three radars ($N_x = 3$), as in the scenario considered in this article, the linearized form is as follows:

$$\begin{cases} \left(\tilde{x}-x_1\right)^2+\left(\tilde{y}-y_1\right)^2-\left(\tilde{x}-x_3\right)^2-\left(\tilde{y}-y_3\right)^2 &= r_{0,1}^2-r_{0,3}^2 \\ \left(\tilde{x}-x_2\right)^2+\left(\tilde{y}-y_2\right)^2-\left(\tilde{x}-x_3\right)^2-\left(\tilde{y}-y_3\right)^2 &= r_{0,2}^2-r_{0,3}^2. \end{cases} \tag{4}$$

Equation (4) can then be rewritten for compactness in matrix notation by defining

$$\mathbf{A} = \begin{bmatrix} 2(x_1-x_3) & 2(y_1-y_3) \\ 2(x_2-x_3) & 2(y_2-y_3) \end{bmatrix} \tag{5}$$

$$\mathbf{b} = \begin{bmatrix} x_1^2-x_3^2+y_1^2-y_3^2+r_{0,3}^2-r_{0,1}^2 \\ x_2^2-x_3^2+y_2^2-y_3^2+r_{0,3}^2-r_{0,2}^2 \end{bmatrix}. \tag{6}$$

Finally, the equation system is solved by an ordinary least squares (OLS) estimation approach. Thus, the target coordinates can be computed as

$$\tilde{\mathbf{x}} = \begin{bmatrix} \tilde{x} \\ \tilde{y} \end{bmatrix} = \left(\mathbf{A}^T\mathbf{A}\right)^{-1}\mathbf{A}^T\mathbf{b} \tag{7}$$

where $(\mathbf{A}^T\mathbf{A})^{-1}\mathbf{A}^T$ is the Moore–Penrose inverse, with more insights provided in [43].

As shown in Fig. 6, with the radar locations known, the Euclidean distance between the dynamic target location and the stationary radars can be recomputed as $|\mathbf{x}_{nx}-\tilde{\mathbf{x}}| = \hat{r}_{0,nx}$, with $\hat{r}_{0,nx}$ the recomputed LOS distance for the node nx. It is assumed that $|\hat{r}_{0,nx}-r_{0,nx}| = \epsilon \to 0$, indicating the multilateration processing error, is close to 0 with $\hat{r}_{0,nx} \approx r_{0,nx}$, which includes the scatterers from different surfaces of a human body. Then, substituting the range $r_{0,nx}$ into (3a), the round-trip range is calculated.

In need of higher order multipath ways, the radar's location can be mirrored on the reflection wall, with the straightforward multipath model assumed and without prior knowledge of the multipath's angle of incidence and reflection required. Mathematically, a reflection on the unit vector $\hat{\mathbf{i}}_x = [1, 0]^T$ is computed since it is assumed that the reflection wall forms

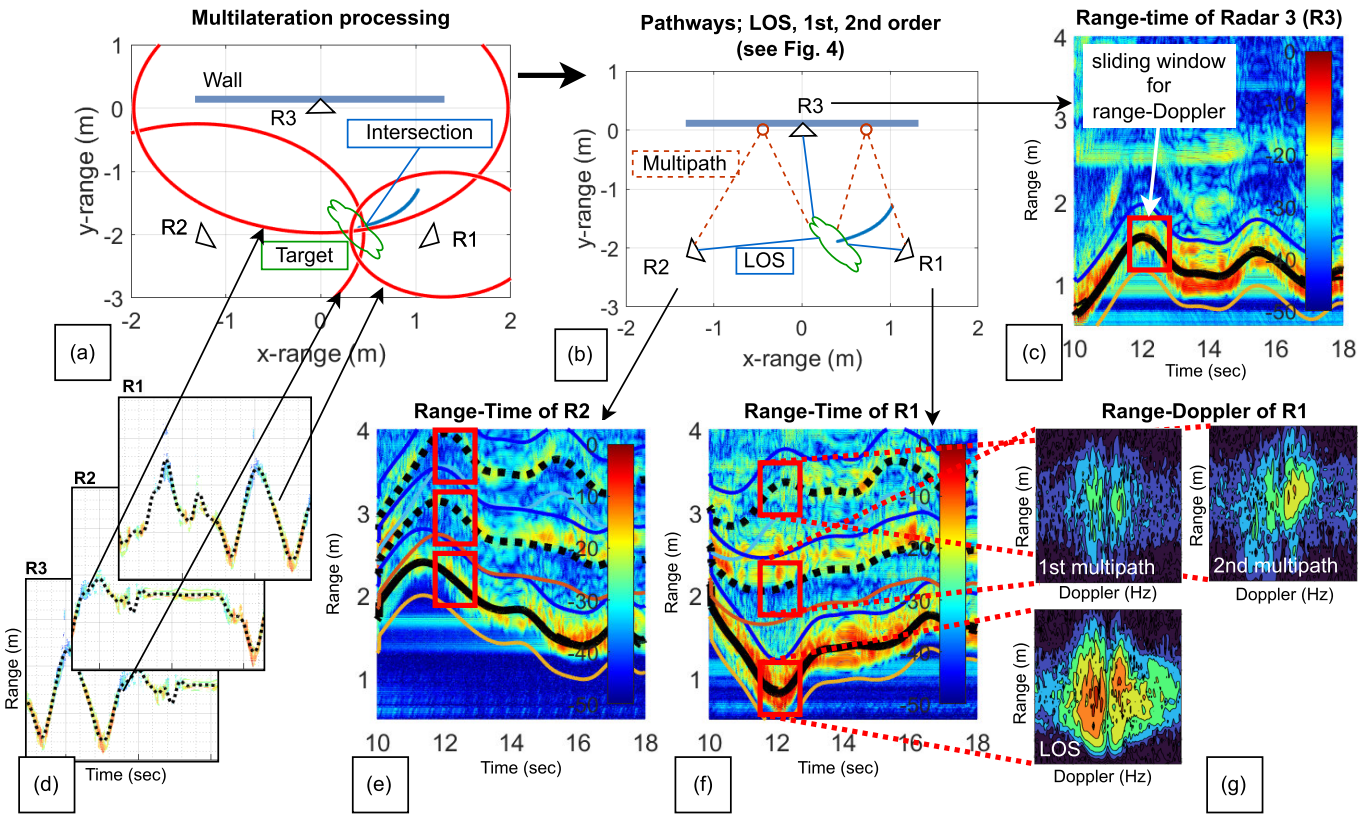

Fig. 6. Flowgraph illustrating the multilateration approach used to determine the target's location and its associated multipath components. In (d), the target's LOS from each radar is depicted, which is essential for (a) multilateration processing. (c), (e), and (f) LOS and multipath components are extracted from the RT images. (g) Computed RD maps for radar 1 (R1). Although RD processing is also carried out for radars R2 and R3, their maps are omitted for brevity.

the coordinate system's x-axis at ordinate 0. Thus, the angle θ between the radar location and the unit vector is needed for the rotation matrix $\mathbf{R}(\beta)$ to compute the mirrored radar location $\mathbf{x}'_{nx}$ as

$$\cos(\theta) = \frac{\mathbf{x}_{nx}\hat{\mathbf{i}}_x}{|\mathbf{x}_{nx}||\hat{\mathbf{i}}_x|} \rightarrow \theta = \cos^{-1}\left(\frac{\mathbf{x}_{nx}\hat{\mathbf{i}}_x}{|\mathbf{x}_{nx}||\hat{\mathbf{i}}_x|}\right) \tag{8a}$$

$$\beta = 2(\pi - \theta) \tag{8b}$$

$$\mathbf{R}(\beta) = \begin{bmatrix} \cos\beta & -\sin\beta \\ \sin\beta & \cos\beta \end{bmatrix} \tag{8c}$$

$$\mathbf{x}'_{nx} = \mathbf{R}(\beta)\mathbf{x}_{nx} = \begin{bmatrix} \cos(\beta)x_{nx} - \sin(\beta)y_{nx} \\ \sin(\beta)x_{nx} + \cos(\beta)y_{nx} \end{bmatrix} \tag{8d}$$

where β is the supplementary angle of 2θ. With this geometrical model, the location of the mirrored radar is obtained with respect to the reflective wall denoted by $\mathbf{x}'_{nx} = [x'_{nx}, y'_{nx}]^T$. The sum of $r'_1 + r_2$ is then simply the Euclidean distance of $|\mathbf{x}'_{nx} - \tilde{\mathbf{x}}| = (r'_1 + r_2)_{nx}$ and can be substituted in (3b) and (3c), with the graphical illustration shown in Fig. 5(b). Finally, the LOS and 1st- and 2nd-order multipath components related to the two radars—R1 and R2—facing the reflective wall are determined.

Furthermore, due to the extended scattering nature of the human body for high-resolution radars, a window of 50 cm width (i.e., the empirically defined shoulder width of an average person) was placed around the target location returned from the multilateration algorithm. This window can be observed by the upper and lower bounds in Fig. 6(c), (e), and (f). Subsequently, the RD domains are extracted using a sliding window technique, exemplified in Fig. 6(g) for radar 1 (R1). Analogous extractions are performed for the remaining radars but are omitted from the visuals for conciseness. These RD domains are utilized as direct inputs for the deep learning network (DL), designated as ML model 2, and for additional feature extraction algorithms such as PCA in the context of ML model 1.

3) Further RD Processing: Earlier in this section, the variables $\Gamma_{0,nx}$, $\Gamma_{1,nx}$, and $\Gamma_{2,nx}$ were introduced to provide the ranges in the RT map associated with the LOS and 1st- and 2nd-order multipath components, respectively. As can be seen in Fig. 6(c), (e), and (f), the ranges of these components change over time, which is the result of the human target moving. Therefore, the variables Γ are dynamically computed for each slow-time hop of 0.20 s (equivalent to 25 samples).

A sliding window with the dimension of 50 cm in range and 0.82 s (100 samples) in slow time is placed for each component (the LOS and 1st- and 2nd-order multipath) at the centroid ranges determined by Γ, as shown in Fig. 6(c), (e), and (f).

In these windows and with the aforementioned slow-time hop size of 0.20 s, a 1 dimensional fast Fourier transform (1D-FFT) in slow-time dimension computes the RD maps to be used for subsequent classification. In the geometry considered, there are seven data domains that can be considered, namely, the 0th (LOS) component and the multipath components of 1st and 2nd orders of the radars R1 and R2, respectively, and the LOS component of R3. These RD maps will contain information on the measured radial velocities of

the human target's body parts with respect to each propagation path, including those paths associated with radars generated virtually through multipath reflections [31].

C. ML Processing for Classification

In this section, two classification approaches are explained. These include ML model 1 [depicted in Fig. 1(e)], that is, a simple SVM or MLP classifier operating on prior extracted principal component analysis (PCA) features. Second, ML model 2, a 12-layer CNN, as shown in Fig. 1(d), is also tested with RD maps as input. The models are rigorously evaluated utilizing an L1Po test that evaluates the performance of the classifiers on data from unseen subjects.

1) Data Preprocessing and Upsampling: Regardless of the applied ML pipeline, the RD data domains are preprocessed before applying PCA feature extraction or passing the images to the CNN. Essentially, the complex RD maps are converted to a magnitude logarithmic scale before resizing them to a 64×64 image size. Furthermore, image normalization to a dynamic range of $\mathbb{R} \in [0, 1]$ is applied [44].

As described in more detail in Section III-A, the dataset [28] considered is unbalanced due to the prevalence of walking and stationary behavior over individual in-place activities such as sitting, bending, or standing. To address the problems of training any classifier with unbalanced datasets, novel techniques have been proposed in the literature, including sampling-based approaches [45] and cost function-based approaches [46]. After analyzing multiple methodologies, SMOTE technique [26] was selected as the data upsampling technique for this work and applied to both the PCA feature vectors used for ML model 1, as well as on RD images directly for ML model 2. The application of SMOTE directly to images, as opposed to feature vectors, is less common in the literature. However, its feasibility has been demonstrated in studies such as [27] and [29]. It is pertinent to mention that SMOTE, when applied prior to classification, is not limited to CNN architectures, but it can be used to upsample image data of minority classes regardless of the subsequent classification algorithm used. An alternative approach can be the generation of synthetic data using a generative adversarial network (GAN), as demonstrated on micro-Doppler spectrograms in [47]; however, this was considered beyond the scope of this article.

2) ML Model 1: ML model 1 consists of the following steps operating on the preprocessed RD images, as shown in Fig. 1(e):

1) PCA feature extraction;
2) feature vector concatenation;
3) SMOTE upsampling (if desired);
4) train, validation, and L1Po test split;
5) classifier (SVM or MLP) $\rightarrow$ prediction and result evaluation.

PCA was chosen to extract features as a powerful, nonparametric tool that can discard irrelevant dimensions and keep the salient features [48] in the data. This was applied on all RD images independently, regardless of whether they were data from the LOS or multipath components. First, the covariance

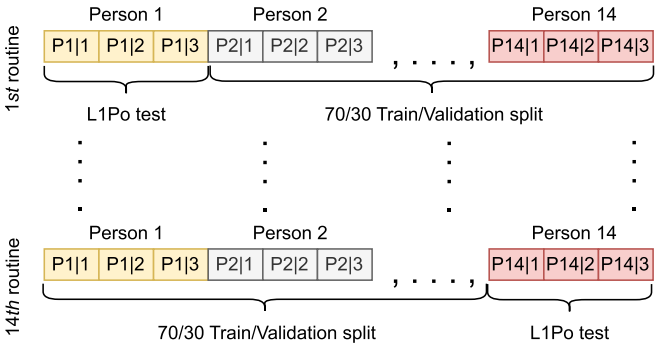

Fig. 7. Training and validation split for the L1Po test, excluding data from one individual (three sequences per person). This process is iterated 14 times, once for each participant, with the classification metrics averaged across all iterations.

matrix is computed as

$$\mathbf{H} = \frac{1}{I}\sum_{i=0}^{I-1}\left(\mathbf{X}_i - \bar{X}_i\right)^T \cdot \left(\mathbf{X}_i - \bar{X}_i\right) \tag{9}$$

with $\mathbf{X}$ and $\bar{X}$ the RD image and the mean image, respectively, both $\in \mathbb{R}^{\eta\times\eta}$ of the dataset size I. Then, eigenvalue decomposition of the covariance matrix $\mathbf{H}$ is performed to compute the eigenvalues λ_i and the eigenvectors contained in $\Phi = [\nu_1, \nu_2, \ldots, \nu_k, \nu_{k+1}, \ldots, \nu_\eta] = [\Phi_k, \nu_{k+1}, \ldots, \nu_\eta]$. Subsequently, the five eigenvectors ($k = 5$) associated with the magnitude of the largest ordered eigenvalues are selected before projecting the original RD image $\mathbf{X}$ on Φ_k to compute the feature matrix, $\upsilon \in \mathbb{R}^{\eta\times k}$ used for classification as, $\upsilon = \mathbf{X}\Phi_k$ [49]. The feature matrix υ for each RD image is flattened to obtain the vector $\tilde{\upsilon} \in \mathbb{R}^{(\eta k\times 1)}$. When multiple radars and/or multipath components are considered, PCA is applied on the RD image of each of the seven data domains and the total feature vector is defined as

$$\Upsilon = \left[\tilde{\upsilon}^T_{R1|0\text{th}}, \tilde{\upsilon}^T_{R1|1\text{st}}, \tilde{\upsilon}^T_{R1|2\text{nd}}, \tilde{\upsilon}^T_{R2|0\text{th}}, \tilde{\upsilon}^T_{R2|1\text{st}}, \tilde{\upsilon}^T_{R2|2\text{nd}}, \tilde{\upsilon}^T_{R3|0\text{th}}\right]^T \tag{10}$$

with $_{R\{\cdot\}|\{\text{Domain}\}}$ indicating radar and domain. The feature vector has a length of $\mathbb{R}^{7\eta k\times 1}$ if all seven data domains are considered or shorter if only a subset of domains is considered. After obtaining the feature vectors with their associated labels, SMOTE can be applied if desired [26].

In terms of training/validation/test data splitting, the L1Po approach is chosen so that data from one participant are held out for testing and the data of the remaining 13 participants is used with a 70/30 training/validation split. This process is then repeated for each participant, as shown in Fig. 7, with the final results averaged across all participants.

The training/validation data are used with an SVM classifier with a radial basis function (RBF) kernel and with an MLP with three hidden units and eight nodes per layer; ReLu activation functions and ADAM optimizer are used for the MLP [50]. Both SVM and MLP are implemented in Python using the Scikit-learn package [51]. The weighted average F1-score and accuracy serve as performance metrics for the validation data and the L1Po test. These metrics are computed and presented in Section III-B1.

TABLE I

MODIFIED CNN ARCHITECTURE PROPOSED BY VANSCHOREN [52] FOR A SIX-CLASS PROBLEM. NOTE: * UP TO SEVEN CHANNELS USED HERE DEPENDING ON THE NUMBER OF INPUT DATA DOMAINS

Layer type	Input	Output
InputLayer	(64, 64, 7)*	(64, 64, 7)*
Conv2D	(64, 64, 7)	(62, 62, 32)
MaxPooling2D	(62, 62, 32)	(31, 31, 32)
Conv2D	(31, 31, 32)	(29, 29, 64)
MaxPooling2D	(29, 29, 64)	(14, 14, 64)
Conv2D	(14, 14, 64)	(12, 12, 128)
MaxPooling2D	(12, 12, 128)	(6, 6, 128)
Conv2D	(6, 6, 128)	(4, 4, 128)
MaxPooling2D	(4, 4, 128)	(2, 2, 128)
Flatten	(2, 2, 128)	(512)
Dropout	(512)	(512)
Dense	(512)	(512)
Dense	(512)	(6)

3) ML Model 2: The pipeline of ML model 2 consists of fewer blocks than ML model 1, shown in Fig. 1(d):

1) SMOTE upsampling (if desired);
2) training, validation, and L1Po test split;
3) CNN classifier → prediction and result evaluation.

The implemented CNN architecture operates directly on the RD image data **X**, and hence, no separate feature extraction is required. Next, a 3rd-order tensor is created as the network's input data by using the matrices **X** of up to seven available data domains by essentially stacking together the RD images of all domains (LOS and/or multipath). The created tensor dimensions can vary within $\in \mathbb{R}^{\eta\times\eta\times\{1,\ldots,7\}}$. In terms of CNN architecture, after empirical tests, the best results were achieved by a 12-layer network (excluding the input layer) inspired by [52]. The Keras network [53] was modified to fit the size of the input data with its architecture shown in Table I.

Simple hyperparameter tuning was performed using an ADAM optimizer [50] with a learning rate found of 0.001 (limits: [0.0001, 0.01]). An early stopping mechanism with a patience cycle of ten epochs based on the validation loss and a maximum of 250 epochs was used. The network stopped training on average at 100 epochs. Furthermore, the dropout layer was set to 0.5 (steps: [0.2, 0.35, 0.5]), with 0.5 being the general maximum probability for a typical network [54].

III. DATASET DESCRIPTION AND RESULTS

In this section, the experimental dataset[1][2] [28] collected to validate the proposed approach is described, together with the results. The dataset's read functions are linked in [28], and [55]. The dataset focuses on single wall reflection, distinguishing it from other publicly available datasets [8], [9], [10], [11], which primarily do not include multipath components. It is demonstrated how the incorporation of information from the multipath components can improve the classification results for continuous HAR.

A. Dataset

Three separate continuous data sequences were recorded for each participant, with the following six classes: 0—*walking with an object*, 1—*walking without an object*, 2—*stationary condition*, 3—*sitting down*, 4—*standing up from sitting*, and 5—*bending from standing*. As is typical for these semirealistic activity sequences, the dataset is initially imbalanced with the majority class 1—*Walking without an object* and the minority class 4—*standing up from sitting*, as illustrated in Fig. 8(b).

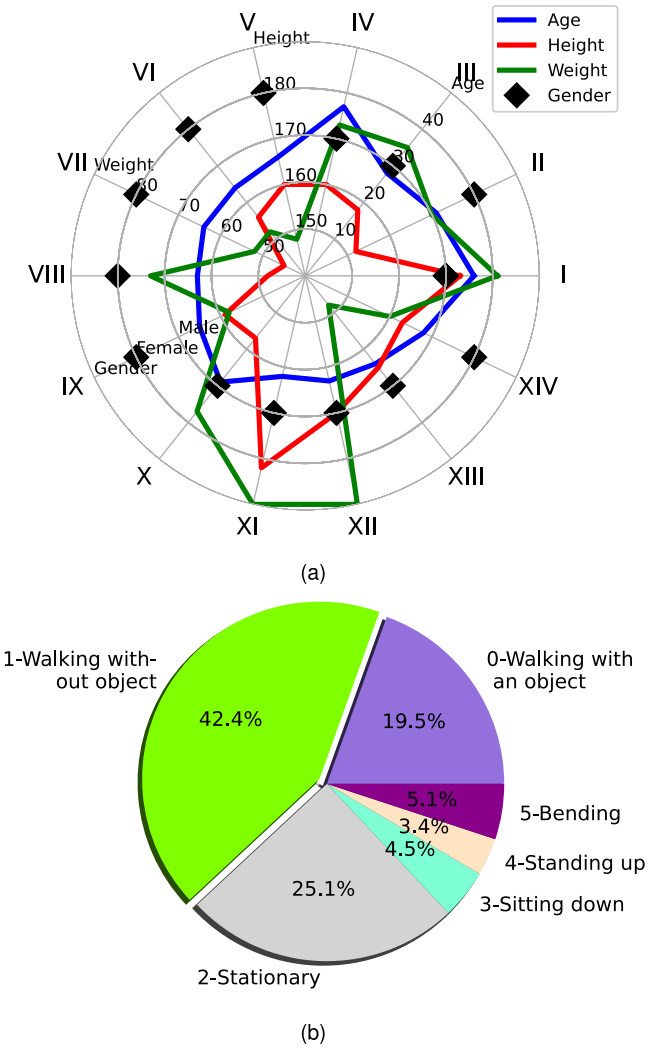

Fig. 8. (a) Metrics for each participant (I, II, ..., XIV), with (b) providing the class distribution within the dataset, with the majority class 1—*walking without an object*—and the minority class 4—*standing up from sitting*.

In total, 14 participants were recorded performing the sequence of activities, one participant at a time. Each sequence has a duration of 1 min. There is a gender-balanced occurrence in the dataset, with seven female and seven male participants with an average of age: 27.1 years (std: 4.7 years), height: 171 cm (std: 10 cm), and weight: 67.6 kg (std: 14.7 kg), with the individuals' characteristics shown in Fig. 8(a).

Three Humatics P410 ultra-wideband (UWB) radar nodes (formerly time domain) are simultaneously employed, with coded waveform capabilities to minimize node interference. The in-phase backscattered signal is recovered through filter banks and the quadrature component is derived using the Hilbert tran sform. Specific radar parameters are detailed in Table II.

The radar nodes are deployed in a triangular geometry, as illustrated in Fig. 5(a). A visual representation of the

[1]https://doi.org/10.4121/e1d6a078-9022-4f48-9aa6-e22389980fee
[2]https://doi.org/10.5281/zenodo.10594435

TABLE II
RELEVANT RADAR PARAMETERS OF THE HUMATICS P410 (FORMERLY PULSON) UWB RADAR NODES [56], [57]

Radar parameters		
Center frequency	f_c	4.3 GHz
Bandwidth	B	2.2 GHz
Range resolution	$r_{res}=\frac{c}{2\cdot B}$	68 mm
slow-time PRF, PRI	f_{PRF}, τ_{PRI}	122 Hz, 8.2 ms
Unambiguous Doppler/velocity	f_{max}, v_{max}	$\pm$61 Hz, $\pm$2.2 m/s
Nominal pulse interval	t_{pulse}	approx. 100 ns
Nominal pulse width	τ_{pulse}	approx. 2 ns
Sampling resolution	T_s	61 ps

experimental setup is given in Fig. 3, where the radar nodes are circled in red and the reflector is marked in green by the rectangle. It should be noted that the brown block in the foreground is a piece of absorbing material, located between the laptop used by the operator and the experimental scene where the participants were moving. Further details about the UWB radar nodes can be found in previous work [40].

B. Experimental Results

First, this section discusses the impact in terms of classification performances of upsampling the experimental dataset [28], a practice applied in other classification contexts to address unbalanced datasets. Second, more novel investigation explores the use of radar multipath propagation to improve classification performances. Therefore, the results of using single radar classification (sR) are compared with those of the entire radar network (aR) that exploits the proposed pipeline with multipath components.

1) Results With Experimental Data Upsampling: Table III presents the results when using the unbalanced dataset as it originates from the data collection, where there are three clear majority classes, namely, 0—*walking with an object*, 1—*walking without an object*, and 2—*stationary condition*. The specific percentage of the sample distribution per class is shown in Fig. 8(b) and is similar to other works in the literature where continuous sequences of activities are analyzed (i.e., [40, Fig. 3]). The prevalence of walking and stationary activities is somewhat expected for semirealistic sequences where the participant moves around a room, whereas the incidence of specific in-place actions, such as sitting, standing, or bending, is instead much lower. Several techniques have been introduced to handle unbalanced data [58], and throughout this work, the SMOTE algorithm was used to generate balanced data for training and validation purposes.

The advantage in classification performance of applying upsampling can be seen in Table III, where the first two rows report classification metrics for the initial unbalanced dataset and the two bottom rows for the upsampled dataset via SMOTE. The table reports the validation results in terms of accuracy and F1-score, as well as the averaged test results for the L1Po approach, for both MLP and SVM classifier using PCA features. It should be noted that for simplicity, PCA features of all seven data domains (*all domains*) were used, such as the LOS and multipath components of R1 and R2,

TABLE III
VALIDATION ACCURACY AND F1-SCORES TOGETHER WITH L1PO RESULTS ACROSS 14 PARTICIPANTS. THE TOP TWO ROWS SHOW THE RESULTS FOR THE INITIAL UNBALANCED DATASET (*Upsampling: None*), AND THE BOTTOM TWO ROWS SHOW THE RESULTS FOR A BALANCED TRAINING/VALIDATION SET USING *SMOTE*. MLP AND SVM CLASSIFIERS WERE TESTED WITH PCA FEATURES

Upsampling	Classif.	Domains	Valid. Acc.	L1Po Acc.	Valid. F1-sc.	L1Po F1-sc.
None	MLP	All domains	71 %	52 %	70 %	51 %
None	SVM	All domains	84 %	61 %	85 %	60 %
SMOTE	MLP	All domains	84 %	58 %	84 %	59 %
SMOTE	SVM	All domains	**89** %	**63** %	**89** %	**64** %

and the LOS of R3. It can be seen that there is a consistent improvement in using a balanced dataset, with L1Po test results reported of +8% using MLP and +4% using SVM. Based on these results, SMOTE is consistently used for all subsequent tests in this study.

2) Selection of Data Domains: Both ML model 1 (PCA features + MLP/SVM classifier) pipeline and ML model 2 (CNN on RD images) pipeline were tested to investigate the multipath's impact on classification performances. First, an exhaustive feature selection (EFS) was performed using the less computationally complex ML model 1 to evaluate variations as a function of the number of PCA features considered when different combinations of data domains are utilized. As discussed in Sections I and II, the chosen radar layout can benefit from up to seven domains, consisting of 3xLOS (3x0th), 2x1st, and 2x2nd order multipath domains. Therefore, 127 domain combinations can be considered for classification, that is, the sum of the binomial coefficient from one domain to seven domains ($m = 7$), calculated by the following equation $127 = \sum_{i=1}^{m} \binom{m}{i}$.

a) Performance analysis evaluated using ML model 1: The combinatorial analysis for the different data domains was computed using the MLxtend [59] package with the MLP classifier operating on the principal component vectors of each domain. In evaluating classification accuracy, the algorithm trains the MLP classifier on every domain combination with a fivefold cross-validation split. The average score with its upper and lower standard deviation values is shown in Fig. 9, starting from 60% accuracy for one domain, up to 83% by using all seven domains combined. In addition, sequential feature selection (SFS) was investigated and equivalent conclusions were drawn that the best classification performance was achieved using the full set of domains, including multipath components.

b) Performance analysis evaluated using ML model 2: As introduced in Section II-C3, ML model 2 is a 12-layer CNN that uses up to seven RD domains as input. The input layer of the network adapts to the number of combined domains, such as with dimensions of 64 × 64 × 7 when all seven domains are used, and 64 × 64 × 3 for just the three LOS domains.

The system's performance for a single radar (sR) is evaluated using only one input domain, namely, the Line-of-Sight (LOS) domain of each radar node. The results of this test are provided in Table IV in the first row, averaged for the

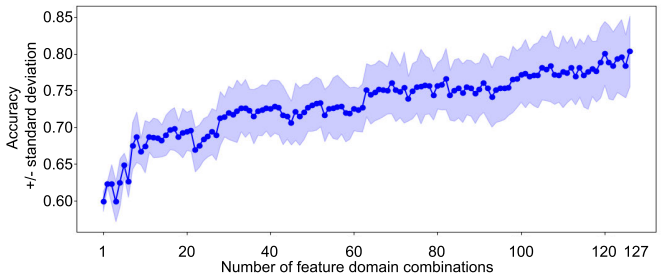

Fig. 9. Accuracy and standard deviation from EFS considering all possible feature combinations using the MLxtend [59] package with the MLP classifier.

three radars considered in this deployment scenario. It can be seen that the model overfits and is not well capable of classifying unseen data, as the L1Po F1-score test of 59% shows. When multipath components are considered using the proposed processing pipeline for a single radar, the results improve, as can be seen in Table IV. Specifically, the L1Po test F1-score improves by 5% and 4%, respectively, with 64% and 63% using a single radar LOS plus its 1st- or 2nd-order multipath component and reaching 65% for both components in addition to the LOS (+6% improvement versus using only the LOS). This appears to suggest that the incorporation of multipath components into the classification process enabled by the proposed pipeline can improve performances, whereby the multipath components allow to gain a multiperspective view on the target from different AoAs.

When all the radars and all their available domains (LOS and multipath domains) are used for classification, the best results are achieved, with an L1Po test F1-score of 70%, averaged over 14 tested individuals. This represents an improvement of +11% with respect to the case of using single radars with only their LOS and +2% with respect to using the network's three LOS domains only without their multipath information (the L1Po test F1-score increases from 68% to 70%).

The training, validation, and L1Po test confusion matrices can be seen in Fig. 10(a)–(c) when all data domains are considered. It should be noted that the training and validation data are balanced via SMOTE, as observable in the matrices in Fig. 10(a) and (b), whereas the L1Po test result in Fig. 10(c) is imbalanced with prevalence of walking movements and stationary status. In addition, for the L1Po case, the matrix is averaged across the results for each of the 14 participants. Class 2—*stationary condition*—is classified with high precision and recall, whereas confusion is observed for classes 0—*walking with an object* versus 1—*walking without an object*. This was already observed in the analysis of their feature distributions using t-distributed stochastic neighbor embedding (t-SNE) [44]. Physically, this similarity can be explained by the fact that in both walking cases, the participants were moving their arms and hands little, even when walking empty-handed. This was due to the fact that the measurement area was relatively small (see Figs. 5(a) and 3), and the participants could only walk a few steps at low speed before changing directions. The rest of the classes, such as 3—*sitting down*, 4—*standing up from sitting*, and 5—*bending from standing*, are the minority classes for

TABLE IV

PERFORMANCE METRICS USING DIFFERENT DOMAINS, NAMELY THREE LOS AND FOUR MULTIPATH DOMAINS, AND THEIR COMBINATIONS WHEN USING THE RADAR NETWORK, DENOTED AS ALL RADARS (aR). PERFORMANCES ARE COMPARED WITH USING ONLY LOS OF SINGLE RADARS (sR), AS WELL AS SINGLE RADARS (sR) WITH ONLY THEIR OWN MULTIPATH COMPONENTS. NOTES #ASSOCIATED CONFUSION MATRICES ARE SHOWN IN FIG. 10. *CLASSIFICATION WITH A SINGLE RADAR HAS A HIGH TRAINING/VALIDATION VARIANCE, LEADING TO LOW PERFORMANCES WITH UNSEEN DATA, AS FOR L1PO F1-SCORE REPORTED

Classifier: CNN	**Upsampling: SMOTE**				**Gain**
Domains	**Valid. Acc.**	**L1Po Acc.**	**Valid. F1-sc.**	**L1Po F1-sc.**	**L1Po F1-sc.**
LOS (Single radar (sR))#	*90 %	59 %	*90 %	59 %	0 %
LOS+1^{st} (sR)	87 %	64 %	87 %	64 %	+5 %
LOS+2^{nd} (sR)	85 %	63 %	85 %	63 %	+4 %
LOS+1^{st}+2^{nd} (sR)	82 %	64 %	82 %	65 %	+6 %
All LOS (all radars (aR))	81 %	81 %	81 %	68 %	+9 %
All domains (aR)#	83 %	**83** %	83 %	**70** %	+11 %

in-place actions. These remain challenging to be classified in a semirealistic continuous sequence of activities, especially when the L1Po approach is used to test performances on unseen participants. However, the proposed method, which allows the exploitation of multipath information in the classification process, is enhancing the performance. Comparing Fig. 10(c) with Fig. 10(d) illustrates the improvement in classification performance for the L1Po test of the best single radar case without multipath. The confusion matrix reveals an increase in accuracy across all classes, particularly the minority ones.

C. Further Discussion

The two radars positioned at the front of the scene, as shown in Fig. 3, are used to observe multipath components of a moving human target. With this placement of the reflector, specifically in this study a 1.8-m-wide reflectors surface, multiple aspect angles of the moving human target can be observed by exploiting multipath components. Such multiaspect views can provide information from diverse scatter points and perspective of the human body and, typically, it is expected that they would enhance the quality of available information and, thus, the classification robustness. Furthermore, this approach has potential applications for viewing obscured parts of a target that normally cannot be seen with only the conventional LOS view.

While the work presented in this article demonstrated the feasibility of identifying multipath components and their usage to improve human activity classification performances, several aspects have to be taken into account for further validation of the proposed method. First, the portability of the method to other environments with their specific clutter, furniture, shape of rooms, and propagation characteristics, such as the electromagnetic parameters of the walls, will affect the multipath components. Considering higher frequencies, these internal wall reflections may become less significant compared to the C-/S-band radar system used for this study,

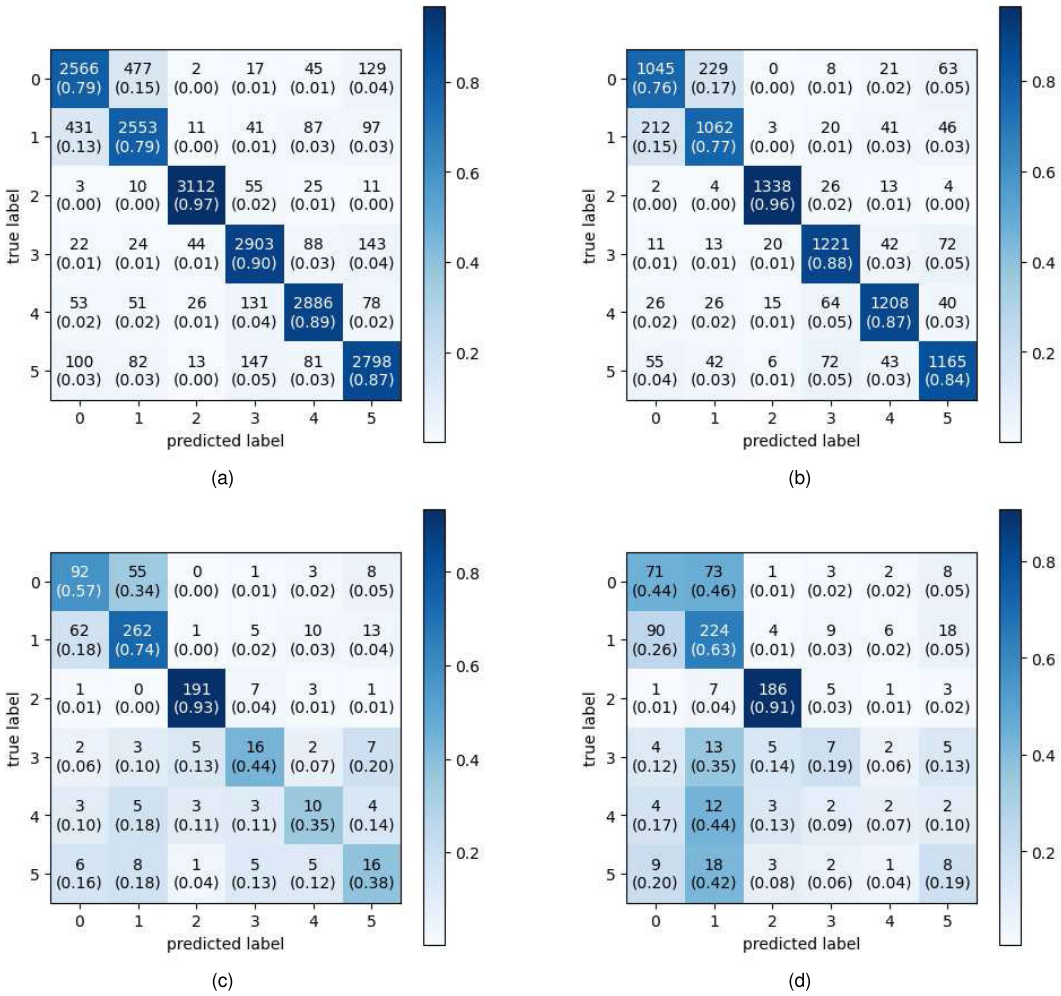

Fig. 10. (a) and (b) Confusion matrices of the CNN classifier listed in Table IV for all domains using all radars for training/validation data, respectively, using SMOTE and the L1PO test result. (c) L1Po testing on all domains using all radars. (d) For comparison, the results of the L1Po test for a single radar. The listed classes are: 0—*walking with an object*, 1—*walking without an object*, 2—*stationary condition*, 3—*sitting down*, 4—*standing up from sitting*, and 5—*bending from standing*.

whereas it is assumed that our reflector's characteristic is more specular than diffuse or heavily affected by the internal reverberation within the material. It is also worth mentioning that this study deliberately confines multipath effects to those caused by a single reflector and 1st- and 2nd-order components. In real-world scenarios, signals might be obscured by obstacles or reflected off multiple reflectors or even larger pieces of furniture. Furthermore, additional complexity in identifying the different propagation paths can happen when exposing the system to a multitarget scenario, where a data association problem must be additionally addressed, leveraging on powerful multitarget tracking algorithms such as MHT.

IV. Conclusion

This article proposed a processing pipeline to exploit multipath in the context of HAR using radar networks. Rather than canceling multipath, as typically wanted for indoor applications, the proposed pipeline enables isolating and tracking the LOS and multipath components related to a moving human target for each radar in the network. Information from the multipath components (e.g., micro-Doppler spectra) is extracted by leveraging on spatial diversity and aspect angles in observations of the same target compared to the LOS component. Importantly, as both—LOS and multipath target observations—are generated from the same physical radar node, the target's multipath signatures are fully coherent with the LOS signature.

The proposed pipeline has been validated with experimental data collected from 14 participants performing continuous sequences of six activities. A network consisting of three pulsed UWB radars was used in an indoor setting. In terms of data processing, it was demonstrated how data upsampling via the SMOTE technique improved the classification results. Notably, SMOTE was directly applied on RD images, which are used further as input for a 12-layer CNN classifier. The results showed that the use of information from multipath components for a single radar node achieves a +6% F1-score improvement for an L1Po test compared to the usage of only its LOS. This improvement increased further to +11% by considering the entire radar network, including its multipath components.

Future work may consider a different deployment geometry for the radar network with respect to the reflector, as well as the usage of MIMO radar nodes that can also provide angular resolution. Furthermore, different classifiers and different

fusion techniques can be investigated to combine the information from the LOS and multipath components differently.

ACKNOWLEDGMENT

The authors are grateful for the constructive discussions with Ignacio Roldan on the implementation of the convolutional neural networks (CNNs) and to all participants in the data collection. They thank Luca Venturino from the Università degli Studi di Cassino e del Lazio Meridionale, Cassino, Italy, for the inspirational discussion at the 2022 IEEE Radar Conference (RadarConf22) in New York, NY, USA, which triggered the idea that ultimately led to this work.

REFERENCES

[1] M. G. Amin, Y. D. Zhang, F. Ahmad, and K. C. D. Ho, "Radar signal processing for elderly fall detection: The future for in-home monitoring," *IEEE Signal Process. Mag.*, vol. 33, no. 2, pp. 71–80, Mar. 2016.

[2] J. Le Kernec et al., "Radar signal processing for sensing in assisted living: The challenges associated with real-time implementation of emerging algorithms," *IEEE Signal Process. Mag.*, vol. 36, no. 4, pp. 29–41, Jul. 2019.

[3] F. Fioranelli, M. Ritchie, and H. Griffiths, "Classification of unarmed/armed personnel using the NetRAD multistatic radar for micro-Doppler and singular value decomposition features," *IEEE Geosci. Remote Sens. Lett.*, vol. 12, no. 9, pp. 1933–1937, Sep. 2015.

[4] S. Zhu, R. G. Guendel, A. Yarovoy, and F. Fioranelli, "Continuous human activity recognition with distributed radar sensor networks and CNN–RNN architectures," *IEEE Trans. Geosci. Remote Sens.*, vol. 60, 2022.

[5] J. Liang and Q. Liang, "Design and analysis of distributed radar sensor networks," *IEEE Trans. Parallel Distrib. Syst.*, vol. 22, no. 11, pp. 1926–1933, Nov. 2011.

[6] F. Luo, E. Bodanese, S. Khan, and K. Wu, "Spectro-temporal modeling for human activity recognition using a radar sensor network," *IEEE Trans. Geosci. Remote Sens.*, vol. 61, 2023.

[7] P. Chen et al., "Multi-view real-time human motion recognition based on ensemble learning," *IEEE Sensors J.*, vol. 21, no. 18, pp. 20335–20347, Sep. 2021.

[8] M. J. Bocus et al., "OPERAnet, a multimodal activity recognition dataset acquired from radio frequency and vision-based sensors," *Sci. Data*, vol. 9, no. 1, pp. 1–18, Aug. 2022. [Online]. Available: https://www.nature.com/articles/s41597-022-01573-2

[9] F. Fioranelli, S. Zhu, and I. Roldan, "Benchmarking classification algorithms for radar-based human activity recognition," *IEEE Aerosp. Electron. Syst. Mag.*, vol. 37, no. 12, pp. 37–40, Dec. 2022.

[10] A. D. Singh, S. S. Sandha, L. Garcia, and M. Srivastava, "RadHAR: Human activity recognition from point clouds generated through a millimeter-wave radar," in *Proc. 3rd ACM Workshop Millimeter-Wave Netw. Sens. Syst.*, New York, NY, USA, NY, USA, 1145, pp. 51–56, doi: 10.1145/3349624.3356768.

[11] M. Chakraborty, H. C. Kumawat, S. V. Dhavale, and A. A. B. Raj, "DIAT-muRadHAR: Radar micro-Doppler signature dataset for human suspicious activity recognition," Tech. Rep., 2022, doi: 10.21227/015m-7415.

[12] Y. Kim and H. Ling, "Human activity classification based on micro-Doppler signatures using a support vector machine," *IEEE Trans. Geosci. Remote Sens.*, vol. 47, no. 5, pp. 1328–1337, May 2009.

[13] S. Z. Gurbuz and M. G. Amin, "Radar-based human-motion recognition with deep learning: Promising applications for indoor monitoring," *IEEE Signal Process. Mag.*, vol. 36, no. 4, pp. 16–28, Jul. 2019.

[14] X. Li, Y. He, and X. Jing, "A survey of deep learning-based human activity recognition in radar," *Remote Sens.*, vol. 11, no. 9, p. 1068, May 2019.

[15] C. Ding et al., "Continuous human motion recognition with a dynamic range-Doppler trajectory method based on FMCW radar," *IEEE Trans. Geosci. Remote Sens.*, vol. 57, no. 9, pp. 6821–6831, Sep. 2019.

[16] I. Ullmann, R. G. Guendel, N. C. Kruse, F. Fioranelli, and A. Yarovoy, "A survey on radar-based continuous human activity recognition," *IEEE J. Microw.*, 2023.

[17] A. Ledergerber and R. D'Andrea, "A multi-static radar network with ultra-wideband radio-equipped devices," *Sensors*, vol. 20, no. 6, p. 1599, Mar. 2020.

[18] I. Milani, C. Bongioanni, F. Colone, and P. Lombardo, "Fusing measurements from Wi-Fi emission-based and passive radar sensors for short-range surveillance," *Remote Sens.*, vol. 13, no. 18, p. 3556, Sep. 2021.

[19] B. Tan, K. Woodbridge, and K. Chetty, "A real-time high resolution passive WiFi Doppler-radar and its applications," in *Proc. Int. Radar Conf.*, 2014, pp. 1–6.

[20] B. Tan, K. Woodbridge, and K. Chetty, "Awireless passive radar system for real-time through-wall movement detection," *IEEE Trans. Aerosp. Electron. Syst.*, vol. 52, no. 5, pp. 2596–2603, Oct. 2016.

[21] Z. Hao, H. Yan, X. Dang, Z. Ma, P. Jin, and W. Ke, "Millimeter-wave radar localization using indoor multipath effect," *Sensors*, vol. 22, no. 15, p. 5671, Jul. 2022.

[22] L. Li and J. L. Krolik, "Simultaneous target and multipath positioning with MIMO radar," in *Proc. IET Int. Conf. Radar Syst.*, Oct. 2012, pp. 1–6.

[23] R. Feng, E. D. Greef, M. Rykunov, H. Sahli, S. Pollin, and A. Bourdoux, "Multipath ghost recognition for indoor MIMO radar," *IEEE Trans. Geosci. Remote Sens.*, vol. 60, 2022.

[24] Y. Yang, C. Hou, Y. Lang, T. Sakamoto, Y. He, and W. Xiang, "Omnidirectional motion classification with monostatic radar system using micro-Doppler signatures," *IEEE Trans. Geosci. Remote Sens.*, vol. 58, no. 5, pp. 3574–3587, May 2020.

[25] X. Qiao, G. Li, T. Shan, and R. Tao, "Human activity classification based on moving orientation determining using multistatic micro-Doppler radar signals," *IEEE Trans. Geosci. Remote Sens.*, vol. 60, 2022.

[26] N. V. Chawla, K. W. Bowyer, L. O. Hall, and W. P. Kegelmeyer, "SMOTE: Synthetic minority over-sampling technique," *J. Artif. Intell. Res.*, vol. 16, pp. 321–357, Jun. 2002.

[27] A. Bhattacharya. (2022). *How to Use Smote for Dealing With Imbalanced Image Dataset for Solving Classification Problems*. [Online]. Available: https://medium.com/swlh/how-to-use-smote-for-dealing-with-imbalanced-image-dataset-for-solving-classification-problems-3aba7d2b9cad

[28] R. G. Guendel, A. Yarovoy, and F. Fioranelli, "Dataset: Continuous human activities utilizing three pulsed radars exploiting multipath," Tech. Rep., 2024, doi: 10.4121/e1d6a078-9022-4f48-9aa6-e22389980fee.

[29] M. S. Reza and J. Ma, "Imbalanced histopathological breast cancer image classification with convolutional neural network," in *Proc. 14th IEEE Int. Conf. Signal Process. (ICSP)*, Aug. 2018, pp. 619–624.

[30] T. Rappaport, *Wireless Communications: Principles and Practice*, 2nd ed. Upper Saddle River, NJ, USA: Prentice-Hall, 5555.

[31] W. A. Holm, *Principles of Modern Radar: Basic Principles* (Radar, Sonar and Navigation). Edison, NJ, USA: IET, 2010.

[32] Y. Lu and Y. Wan, "PHA: A fast potential-based hierarchical agglomerative clustering method," *Pattern Recognit.*, vol. 46, no. 5, pp. 1227–1239, May 2013.

[33] M. Subramaniam, R. Tharmarasa, M. Pelletier, and T. Kirubarajan, "Multipath-assisted multitarget tracking using multiframe assignment," *Proc. SPIE*, vol. 7445, p. 74450, May 1117.

[34] T. Dogaru, C. Sentelle, G. Gennarelli, and F. Soldovieri, *Radar for Indoor Monitoring*. Boca Raton, FL, USA: CRC Press, 2017.

[35] M. Mucientes and W. Burgard, "Multiple hypothesis tracking of clusters of people," in *Proc. IEEE/RSJ Int. Conf. Intell. Robots Syst.*, Oct. 2006, pp. 692–697.

[36] S. Chang, M. Wolf, and J. W. Burdick, "An MHT algorithm for UWB radar-based multiple human target tracking," in *Proc. IEEE Int. Conf. Ultra-Wideband*, Sep. 2009, pp. 459–463.

[37] A. Distante and C. Distante, *Handbook of Image Processing and Computer Vision: Volume 3: From Pattern to Object*, vol. 3. Cham, Switzerland: Springer, 2020.

[38] J. Luiten et al., "HOTA: A higher order metric for evaluating multi-object tracking," *Int. J. Comput. Vis.*, vol. 129, no. 2, pp. 548–578, Feb. 2021.

[39] G. Bonaccorso, *Machine Learning Algorithms : Popular Algorithms for Data Science and Machine Learning*, 2nd ed. Birmingham, U.K.: Packt Publishing, 2018.

[40] R. G. Guendel, F. Fioranelli, and A. Yarovoy, "Distributed radar fusion and recurrent networks for classification of continuous human activities," *IET Radar, Sonar Navigat.*, vol. 16, no. 7, pp. 1144–1161, Jul. 2022.

[41] P. Setlur, M. Amin, and F. Ahmad, "Multipath model and exploitation in through-the-wall and urban radar sensing," *IEEE Trans. Geosci. Remote Sens.*, vol. 49, no. 10, pp. 4021–4034, Oct. 2011.

[42] P. Setlur, G. E. Smith, F. Ahmad, and M. G. Amin, "Target localization with a single sensor via multipath exploitation," *IEEE Trans. Aerosp. Electron. Syst.*, vol. 48, no. 3, pp. 1996–2014, Jul. 2012.
[43] J. Zhou and J. Shi, "RFID localization algorithms and applications—A review," *J. Intell. Manuf.*, vol. 20, pp. 695–707, Apr. 2009.
[44] A. Geron, *Hands-on Machine Learning With Scikit-Learn, Keras, and TensorFlow: Concepts, Tools, and Techniques to Build Intelligent Systems*, 2nd ed. Sebastopol, MA, USA: O'Reilly Media, 5555.
[45] N. Japkowicz and S. Stephen, "The class imbalance problem: A systematic study," *Intell. Data Anal.*, vol. 6, no. 5, pp. 429–449, Jan. 2002.
[46] M. Pazzani, C. Merz, P. Murphy, K. Ali, T. Hume, and C. Brunk, "Reducing misclassification costs," in *Machine Learning Proceedings 1994*. San Mateo, CA, USA: Morgan Kaufmann, 1994, pp. 217–225.
[47] B. Erol, S. Z. Gurbuz, and M. G. Amin, "Motion classification using kinematically sifted ACGAN-synthesized radar micro-Doppler signatures," *IEEE Trans. Aerosp. Electron. Syst.*, vol. 56, no. 4, pp. 3197–3213, Aug. 2020.
[48] B. G. Mobasseri and M. G. Amin, "A time-frequency classifier for human gait recognition," *Proc. SPIE*, vol. 7306, May 1117, Art. no. 730628.
[49] M. G. Amin and R. G. Guendel, "Radar human motion recognition using motion states and two-way classifications," in *Proc. IEEE Int. Radar Conf. (RADAR)*, Apr. 2020, pp. 1046–1051.
[50] D. P. Kingma and J. Ba, "Adam: A method for stochastic optimization," 2014, *arXiv:1412.6980*.
[51] F. Pedregosa et al., "Scikit-learn: Machine learning in Python," *J. Mach. Learn. Res.*, vol. 12, pp. 2825–2830, Nov. 2011.
[52] J. Vanschoren. *Machine Learning for Engineers, Lecture 9: Convolutional Neural Networks*. Accessed: May 1, 2023. [Online]. Available: https://ml-course.github.io/
[53] F. Chollet. (2015). *Keras*. [Online]. Available: https://keras.io
[54] N. Srivastava, G. Hinton, A. Krizhevsky, I. Sutskever, and R. Salakhutdinov, "Dropout: A simple way to prevent neural networks from overfitting," *J. Mach. Learn. Res.*, vol. 15, pp. 1929–1958, Sep. 2014.
[55] R. Guendel, "Rgundel/public_multipath_data_read: Initial release," Tech. Rep., 2024, doi: 10.5281/zenodo.10594435.
[56] T. Truong, "Design of an ultra-wideband frequency system for non-destructive root imaging," M.S. thesis, Univ. Saskatchewan, 2018. [Online]. Available: https://harvest.usask.ca/handle/10388/8505
[57] A. Petroff, "Ultra-wideband: A tool for teaching undergraduates," in *Proc. IEEE Int. Conf. Ultra-WideBand (ICUWB)*, Sep. 2014, pp. 368–373.
[58] H. He and E. A. Garcia, "Learning from imbalanced data," *IEEE Trans. Knowl. Data Eng.*, vol. 21, no. 9, pp. 1263–1284, Sep. 2009.
[59] S. Raschka, "MLxtend: Providing machine learning and data science utilities and extensions to Python's scientific computing stack," *J. Open Source Softw.*, vol. 3, no. 24, p. 638, Apr. 2018.

Ronny Gerhard Guendel (Graduate Student Member, IEEE) received the Diploma-Engineering [Dipl.-Ing. (FH)] degree in automotive electronics from the University of Applied Sciences Zwickau, Zwickau, Germany, in 2017, the Master of Science degree in signal processing and communications from Villanova University, Villanova, PA, USA, in 2019, and the Ph.D. degree from the Delft University of Technology, Delft, The Netherlands, in November 2023.

He worked at the Fraunhofer Institute for Machine Tools and Forming Technology (IWU), Chemnitz, Germany. From 2017 to 2018, he was with Villanova University, as a Fulbright Scholar in electrical engineering. During the summer of 2018, he worked on vehicular wireless communications at the Vodafone Chair, Dresden, Germany, guided by Prof. Gerhard Fettweis. From 2018 to 2019, the Center for Advanced Communications, Villanova University, offered him a research assistantship under Dr. Moeness G. Amin, focusing on continuous activity classification. His research interests include monitoring continuous human activities in range and time beyond micro-Doppler using distributed radar sensor networks and classification for human signature analysis applied to healthcare and security.

Nicolas C. Kruse (Graduate Student Member, IEEE) received the B.Sc. degree in applied physics from the Delft University of Technology, Delft, The Netherlands, in 2017, and the M.Sc. degree in theoretical physics from the University of Groningen, Groningen, The Netherlands, in 2020.

He joined the Microwave Sensing, Systems, and Signals Group, Delft University of Technology, in March 2021, where he is currently researching the classification of continuous human activities.

Francesco Fioranelli (Senior Member, IEEE) received the Laurea (B.Eng., cum laude) and Laurea Specialistica (M.Eng., cum laude) degrees in telecommunication engineering from Università Politecnica delle Marche, Ancona, Italy, in 2007 and 2010, respectively, and the Ph.D. degree from Durham University, Durham, U.K., in 2014.

He was an Assistant Professor with the University of Glasgow, Glasgow, U.K., from 2016 to 2019, and a Research Associate with University College London, London, U.K., from 2014 to 2016. He is currently an Associate Professor at the Delft University of Technology, Delft, The Netherlands. He has authored over 140 publications between book chapters, journal articles, and conference papers, and edited the book *Micro-Doppler Radar and Its Applications* (IET-Scitech, 2020). His research interests include the development of radar systems and automatic classification for human signatures analysis in healthcare and security, drones and unmanned aerial vehicle (UAV) detection and classification, automotive radar, wind farm, and sea clutter.

Mr. Fioranelli received three best paper awards.

Alexander Yarovoy (Fellow, IEEE) received the Diploma degree (Hons.) in radiophysics and electronics and the Candidate Phys. and Math.Sci. and Doctor Phys. and Math.Sci. degrees in radiophysics from Kharkov State University, Kharkiv, Ukraine, in 1984, 1987, and 1994, respectively.

In 1987, he joined the Department of Radiophysics, Kharkov State University, as a Researcher, where he became a Full Professor in 1997. From September 1994 to 1996, he was with the Technical University of Ilmenau, Ilmenau, Germany, as a Visiting Researcher. Since 1999, he has been with the Delft University of Technology, Delft, The Netherlands, where he has been leading the Chair of Microwave Sensing, Systems and Signals since 2009. He has authored and coauthored more than 450 scientific or technical articles, six patents, and 14 book chapters. His main research interests are in high-resolution radar, microwave imaging, and applied electromagnetics (in particular, ultra-wideband (UWB) antennas).

Prof. Yarovoy was a recipient of the European Microwave Week Radar Award for the paper that best advances the state-of-the-art in radar technology in 2001 (together with L. P. Ligthart and P. van Genderen) and in 2012 (together with T. Savelyev). In 2010 together with D. Caratelli, he got the Best Paper Award of the Applied Computational Electromagnetic Society (ACES). He served as the Chair and the TPC Chair for the 5th European Radar Conference (EuRA'08), Amsterdam, The Netherlands, and the Secretary of the 1st European Radar Conference (EuRAD'04), Amsterdam. He also served as the Co-Chair and the TPC Chair for the Xth International Conference on GPR (GPR2004), Delft. He served as an Associate Editor for the *International Journal of Microwave and Wireless Technologies* from 2011 to 2018 and a Guest Editor for five special issues of IEEE TRANSACTIONS and other journals. From 2008 to 2017, he served as the Director for the European Microwave Association (EuMA).